Acta Geodyn. Geomater., Vol. 22, No. 3 (219), 317–332, 2025
DOI: 10.13168/AGG.2025.0022
journal homepage: https://www.irsm.cas.cz/acta

ORIGINAL PAPER

GRAIN BREAKAGE IN SHEAR BANDS AND ITS EFFECT ON THE PERMEABILITY DECREASE OF GRANULAR MATERIAL SPECIMENS DURING TRIAXIAL LOADING

Chahra BENAMMAR [1], Sadok FEIA [1] , Abdelhak KHECHAI [1] *, Sidali DENINE [2] and Noureddine DELLA [3]

[1] *Laboratory of Research in Civil Engineering, Mohamed Khider University of Biskra, Biskra, Algeria*
[2] *Laboratory of materials Science and Environment (LMSE), Civil Engineering Department, University Center of Tipaza, Tipaza, Algeria*
[5] *Laboratory of materials Science and Environment (LMSE), Civil Engineering Department, Hassiba Benbouali University of Chlef, Chlef, Algeria*

**Corresponding author's e-mail:* a.khechai@univ-biskra.dz

ARTICLE INFO

Article history:
Received 2 December 2024
Accepted 11 July 2025
Available online 18 August 2025

Keywords:
Permeability
Triaxial loading
Fine particles production
Grain breakage
Density
Shear band

ABSTRACT

This paper aims to achieve an experimental study on changes in permeability of non-cemented soils during shear. In petroleum engineering applications when fluid is injected under pressure in unconsolidated oil reservoir sands, it alters the stress state, particularly near the injection site, potentially increasing permeability due to dilatancy. Strain localization in shear bands near the injection well can affect porosity, which may either increase in the case of a band dilating or decrease due to grain breakage. The present study examines the effect of several parameters on grain breakage and permeability of sheared specimens using Triaxial loading on sieved sand (opening of 125µm) with varying densities (medium density ID = 0.5, moderately dense ID = 0.7, and dense ID = 0.9). The experimental results showed a reduction in permeability after shearing despite the increase in the total void ratio in the dilatancy phase. This decrease in permeability was attributed to grain breakage specifically within the shear band. A key methodological advancement of this study is the use of specimen freezing after shearing to preserve the internal structure. This technique enabled precise cutting of the shear band, allowing for conducted necessary tests and investigate more closely the factors influencing the recorded responses. The grain size distribution analysis carried out on the three parts of the specimen (the bottom, the shear band and the top of the specimen), clearly indicates that the production of fine particles is primarily localized at the shear band. Permeability tests conducted on this same band after triaxial test revealed a decrease in the permeability despite the increase in the global void ratio.
These findings have important practical implications for petroleum engineering and geotechnical applications. Understanding how grain breakage affects permeability can improve predictions of fluid flow in reservoir sands, optimize injection strategies, and mitigate potential permeability losses due to fine particle migration. This study provides a more comprehensive framework for evaluating permeability evolution in unconsolidated formations under shear stress, offering valuable guidance for reservoir management and enhanced oil recovery techniques.

1. INTRODUCTION

Grain breakage has considerable effects on the mechanical behavior of granular soils, which significantly influences the permeability pattern. This phenomenon has been a common interest within several fields, such as geotechnical and petroleum engineering, which has stimulated extensive research at both macroscopic and microscopic scales. In these structures, under certain stress conditions, inter-granular contact forces may exceed grains strength, leading to grain breakage phenomenon and implies a reduction in grain size with varying levels (Turcotte, 1986; Sammis et al., 1986; Coop et al., 2004; Feia et al., 2016).

Understanding behavior at the continuum level requires knowledge of the origin at the particle level and its interactions with the surrounding environment. This connection has been explored by several researchers using multi-scale approaches to enhance knowledge of granular soils and predict their behavior (Bolton et al., 2008; Ando et al., 2013; Karatza, 2017). They have highlighted that the essential factor determining the response of these granular soils is the progressive evolution of their particle size distribution, which strongly depends on consolidation pressure, as well as other factors conditioning this evolution, such as angularity, mineralogical nature, and consequently resistance to breakage, particle size, and initial density.

Significant experimental results have developed some basics of numerical modelling in order to formulate the behavior laws that can provide unpredictable behavioral responses of these soils (Bolton et al., 2008; Wang et al., 2011; Salami et al., 2015). Several studies were explored the crack mechanisms using X-ray tomography (Ando et al., 2013; Zaho et al., 2015; Alikarami et al., 2015; Karatza et al., 2017). This technique is an ideal tool to allow specimens to be imaged non-destructively as they undergo different deformation mechanisms and obtain microscopic-scale explanations for macroscopic-scale responses. Ando et al. (2013),

Cite this article as: Benammar C, Feia S, Khechai A, Denine S, Della N: Grain breakage in shear bands and its effect on the permeability decrease of granular material specimens during Triaxial loading. Acta Geodyn. Geomater., 22, No. 3 (219), 317–332, 2025. DOI: 10.13168/AGG.2025.0022

through this measurement tool, were able to capture images illustrating different stages of grain factures of angular sand under high confinement pressure (7000 kPa). Primarily concentrated within the shear band.

Grain breakage is directly linked to volumetric deformation (Coop et al., 2004; Wang and Yan, 2011; Karatza et al., 2019), suppressing dilatancy potential in granular soils (Arslan et al., 2009; Alikarami et al., 2015), and causes the translation of critical state line downwards (Kikumoto, et al., 2010). These changes significantly affect porosity and permeability (Karatza et al., 2017). Feia et al. (2016) observed that permeability decreases during shearing phase, even with an increase in the total porosity. Regardless of the stress path followed (conventional or inclined), permeability reduction follows a two-slope curve (slow decrease followed by rapid one after formation of shear band), explained by the introduction of fines primarily within the shear band due to grain breakage.

Understanding permeability changes is critical for geotechnical application, such as mitigating plugging during water injection in oil wells. Several researchers have attempted to link soil permeability to its grain size distribution (Hazen, 1911; Terzaghi, 1925; Masch and Denny, 1966). Building upon the fractal concept developed by Mandelbrot (1982), Boadu (2000) introduced a new model based on soil grain size distribution using fractal dimension and distribution entropy, while considering other parameters such as fines content, porosity, and density. Boadu (2001) found that permeability decreases with an increase in fines content up to a critical threshold. Beyond this value, the coefficient *k* becomes insensitive to variations in the fine particle percentage.

Other researchers (Ovalle, 2013; Salami et al., 2015) have relied on energetic approaches based on Griffith's theory (1921), experimental correlations between plastic work and the fracture rate have been developed by Ovalle et al. (2013).

Artificial intelligence has also found its utility in the field of geomaterials. Through machine learning (ML), Wu and Wang (2021) employed an artificial neural network (ANN) model based on Discrete Element Method (DEM) simulation to predict the anisotropy of the contact force chain (CFC) during shear. They observed that the combination of particle size and coordination number has a predominant influence on estimating the CFC, and a high frequency of contact gain and loss occurs within the shear band, indicating an unstable environment conducive to grain fragmentation. The anisotropic distribution of contact forces suggests that some particles experience higher loads than others, thereby increasing the risk of breakage.

Despite extensive research, significant gaps remain in understanding permeability changes due to grain breakage, particularly in relation to evolving particle size distributions, localized fines migration, and their influence on macroscopic hydraulic properties. This study aims to address these gaps by investigating the effect of grain breakage on the physico-mechanical behavior of siliceous sand, including strength, volumetric deformation, and permeability. A consolidated drained (CD) triaxial test will be conducted under different confining pressures (100, 200, 400, 600, and 800 kPa) and densities (ID = 0.5, 0.7, and 0.9). The particle size analysis conducted after shearing on the three parts of the specimen (the bottom, the shear band, and the top of the specimen), revealed that the grain breakage phenomenon is primarily localized within the shear band.

To enhance understanding, this study will focus on detailed shear band analysis. Freezing the specimen post-shearing has been identified as the optimal preservation method, facilitating precise cutting and examination of the shear band. This approach will allow a closer investigation of factors influencing permeability changes due to grain breakage, addressing gaps in current literature and improving predictive models for permeability evolution in granular soils.

2. EXPERIMENTAL PROGRAM

2.1. MATERIALS

The material tested in this work is *Oued z'hor* sand from *the Skikda* region, Algeria. This sand is characterized by sub-rounded grains, and is known as poorly graded clean sand, which consists mainly of silica grains (99 %). Figure 1 shows a view with binocular microscope of the tested sand and gives a clear idea of the grain shape.

The chemical and physical properties are presented in Tables 1 and 2, respectively. In Table 2, e_{min} and e_{max} were measured according to ASTM standards D4253 and D4254.

Table 1 Results of chemical analysis of *Oued* Z*'hor* sand.

Designation	Results (%)
$CaCO_3$	--
CaO	0.80
Al_2O_3	2.36
Fe_2O_3	1.15
SiO_2	94.09
MgO	0.14
Na_2O	0.2
Cl	--
K_2O	0.58
SO_3	0.01

Table 2 Physical characteristics of *Oued* Z*'hor* sand.

Designation	D50	Cu	Distribution	emin	emax	Angularity	ρs (gr/cm3)
Oued Z'hor sand	0.34	1.44	uniform	0.64	0.92	Sub-round	2.68

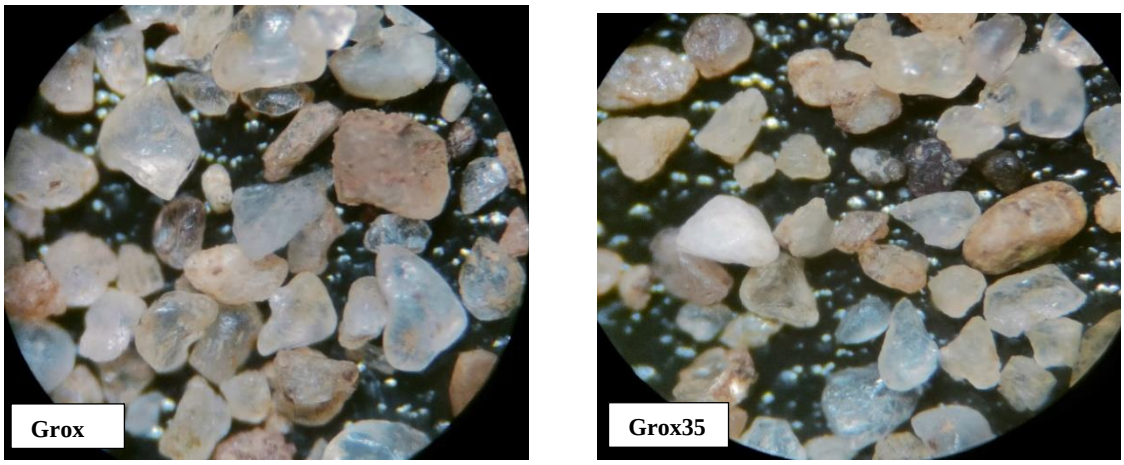

Fig. 1 View with binocular microscope.

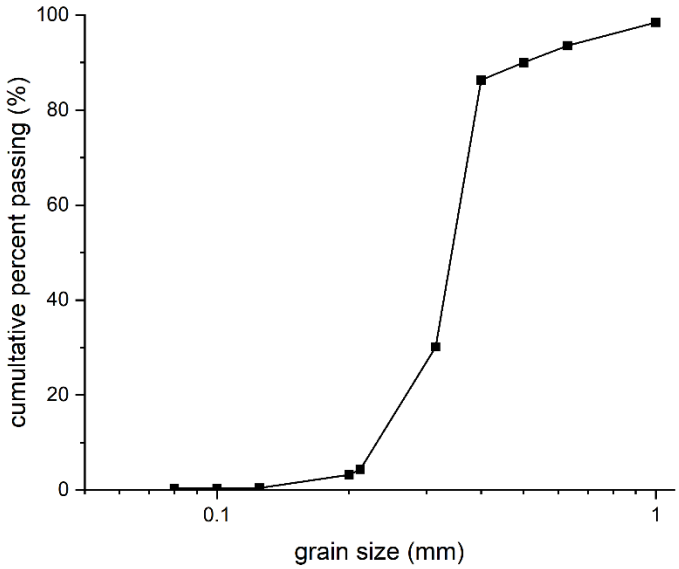

Fig. 2 Grain size distribution of the tested sand (sieved at 0.125 mm).

The grain size distribution curve of the tested sand is shown in Figure 2.

To measure the quantity of fine particles generated during the test, the sand underwent sieving using a sieve with an aperture size of 0.125 mm.

2.2. EXPERIMENTAL DEVICE

Shear tests in consolidated drained (CD) conditions using the Triaxial setup (see Fig. 3), were conducted on each sand sample prepared at different densities (medium $ID_1 = 0.5$, moderately dense, $ID_2 = 0.7$, and dense $ID_3 = 0.9$) and subjected to confinement stresses of ($\sigma_1 = 100$ kPa, $\sigma_2 = 200$ kPa, $\sigma_3 = 400$ kPa, $\sigma_4 = 600$ kPa and $\sigma_5 = 800$ kPa).

These tests were followed by grain size analysis to quantify the mass of fine particles produced after shearing. Additionally, permeability measurements are conducted using the Mariotte tube method (see Fig. 4), which allows for a constant head, to assess the effect of grain breakage on changes in permeability.

2.3. EXPERIMENTAL SETUP AND PROCEDURES

The triaxial shear tests were conducted in a cylindrical cell with diameter D = 70 mm and a height H = 140 mm (see Fig. 5(a)). Specimens were prepared layer by layer to achieve the target density value within a mold containing a membrane, placed directly on the lower base of the triaxial cell. A vacuum of 10 kPa to 20 kPa was applied inside the specimen throughout the assembly process. After setting up the cylindrical chamber, the cell was filled with de-aired water, allowing air to escape through the purge system located on the lid. The first pressure stage was then applied to the cell to initiate the saturation phase. Before loading, the sample was saturated for each confining pressure. Saturation was

Fig. 3 Triaxial Apparatus.

Fig. 4 Mariotte tube.

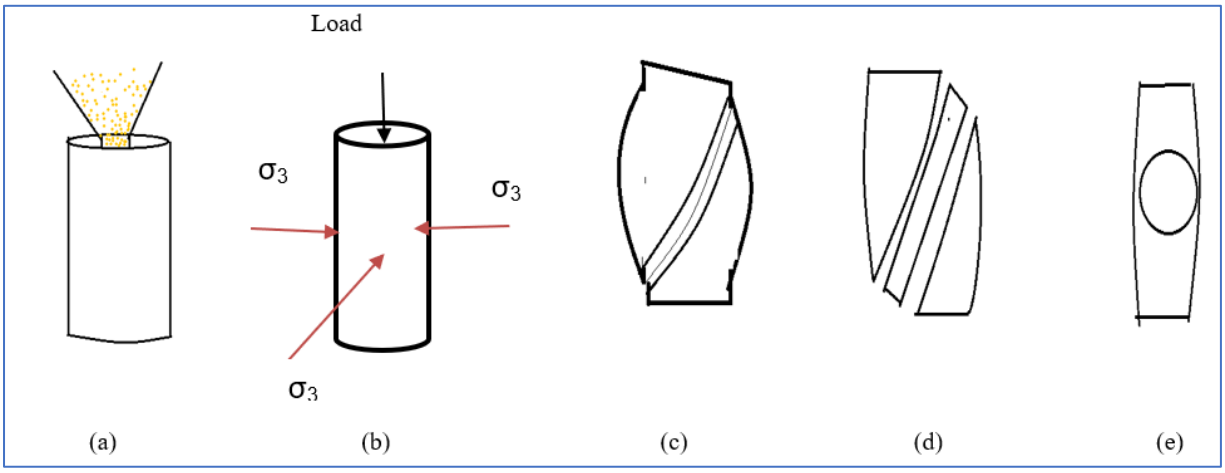

Fig. 5 Schematic representation of experimental setup. (a) specimen preparation, (b) loading, (c) freezing, (d) cutting of shear band, (e) sampling for the permeability test.

controlled by measuring the Skempton B coefficient, which represents the ratio between the change in pore pressure and the change in applied cell pressure. In this study, all B coefficient values were above 0.90.

At the end of consolidation, the drainage circuits remain open and shearing begins at the rate of 1 mm/min under various confining pressures (σ_1 = 100 kPa, σ_2 = 200 kPa, σ_3 = 400 kPa, σ_4 = 600 kPa and σ_5 = 800 kPa), for the different density values. In order to enable the continuation of subsequent tests, namely, grain size analysis and permeability, freezing the specimens was the only means to preserve the shear band (see Fig. 5(c)). The process of artificial soil freezing was initially employed by miners for shaft sinking, but it was only after the last world war that its field of application expanded, and substantial progress was made in theoretical-experimental research and technology.

Freezing the specimen after each test allowed us to conduct permeability tests and grain size analysis directly on the shear band facilitated by its meticulous cutting (see Fig. 5(d)).

The sampling for conducting the permeability test using the Mariotte tube is taken directly from the shear band (see Fig. 5 (e)) just after cutting, the test is carried out only after thawing the sample.

To better illustrate these steps, Figure 6 presents some photos for each step.

2.4. EXPERIMENTAL PROGRAM

Table 3 provides a summary of the main parameters of the experimental program. All samples have been subjected to the same maximum axial strain around 18 %.

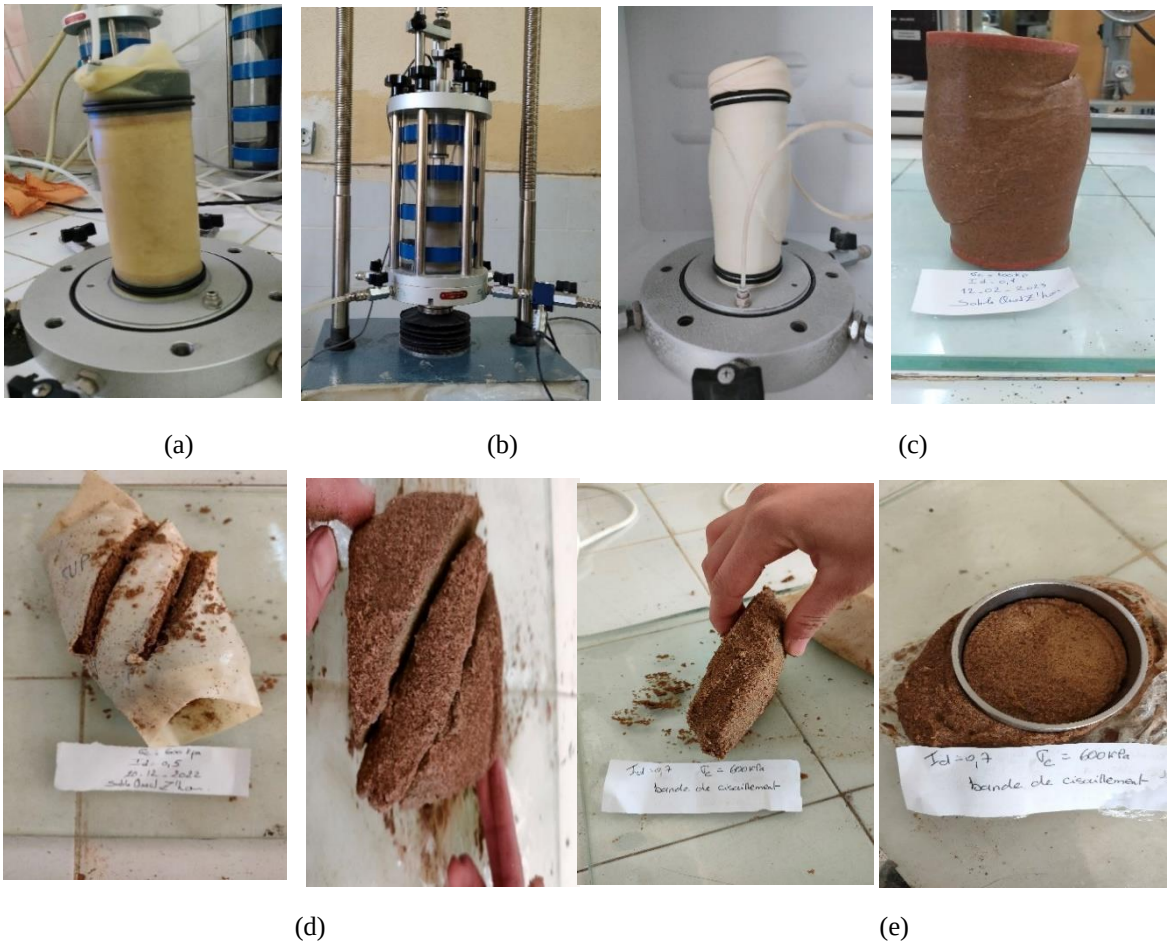

(a) (b) (c)

(d) (e)

Fig. 6 Specimen preparation before and after test. (a) specimen preparation, (c) freezing, (d) cutting of shear band, (e) sampling for the permeability test.

Table 3 Experimental program.

Tests	σ'_c (kPa)	Void ratio (e)	ID
OZ11		0.67	0.9
OZ12	100	0.72	0.7
OZ13		0.78	0.5
OZ21		0.67	0.9
OZ22	200	0.72	0.7
OZ23		0.78	0.5
OZ41		0.67	0.9
OZ42	400	0.72	0.7
OZ43		0.78	0.5
OZ61		0.67	0.9
OZ62	600	0.72	0.7
OZ63		0.78	0.5
OZ81		0.67	0.9
OZ82	800	0.72	0.7
OZ83		0.78	0.5

3. EXPERIMENTAL RESULTS

3.1. TYPICAL RESPONSE

In this section, we first present in detail the results of a typical test performed on dense sand (ID = 0.9) OZ41, under 400 kPa confining pressure, then the influence of other parameters will be discussed.

A classical response of dense sand is observed in Figure 7, with a quasi-linear stress evolution at low strains, followed by a nonlinear evolution up to a maximum deviatoric stress, and finally a softening phase during which the deviator slowly decreases to an ultimate state (Fig. 7a). Two shear strengths are observed: a maximum strength, known as the peak strength, and a strength at large deformation, known as the critical state strength.

The sharp decrease of the deviator in the post-peak regime is associated with the development of a well-defined shear plane within the specimen (Fig. 8). The volumetric response is presented in Figure 7(b). This response exhibits a contracting phase followed by a dilating one.

The granulometric analysis performed on the three parts of the sample (the bottom, the shear band and the top of the specimen), reveals that the fine particles are primarily located at the shear band (see Fig. 9). Initially, the sand was sieved at 0.125 mm to better assess the evolution of fine particles. The determination of fines particles is based on this sieve opening.

The granulometric analysis performed on the three parts of the sample (the bottom, the shear band and the top of the specimen), reveals that the fine particles are primarily located at the shear band (see Fig. 9). Initially, the sand was sieved at 0.125 mm to better assess the evolution of fine particles. The determination of fines particles is based on this sieve opening.

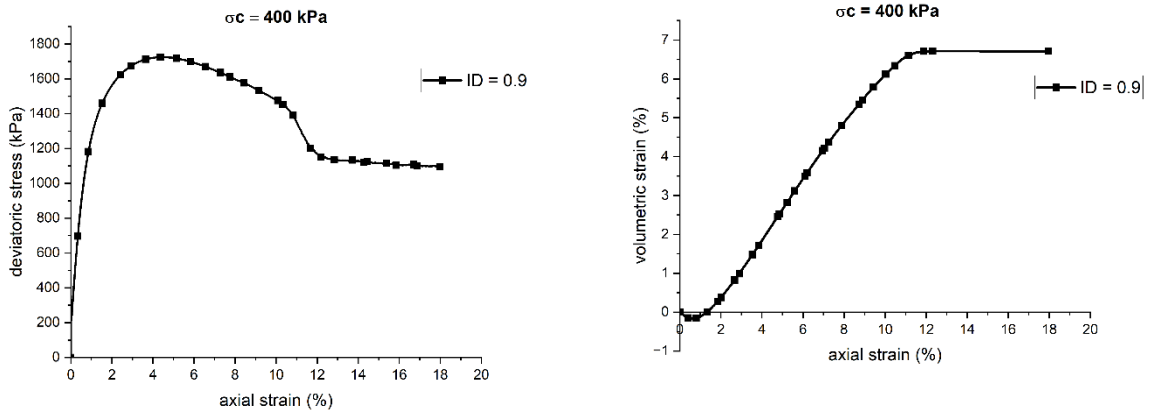

(a) (b)

Fig. 7 (a) Deviatoric stress – axial strain curve (b) volumetric strain-axial strain.

Fig. 8 Shear plane observed on the test OZ41.

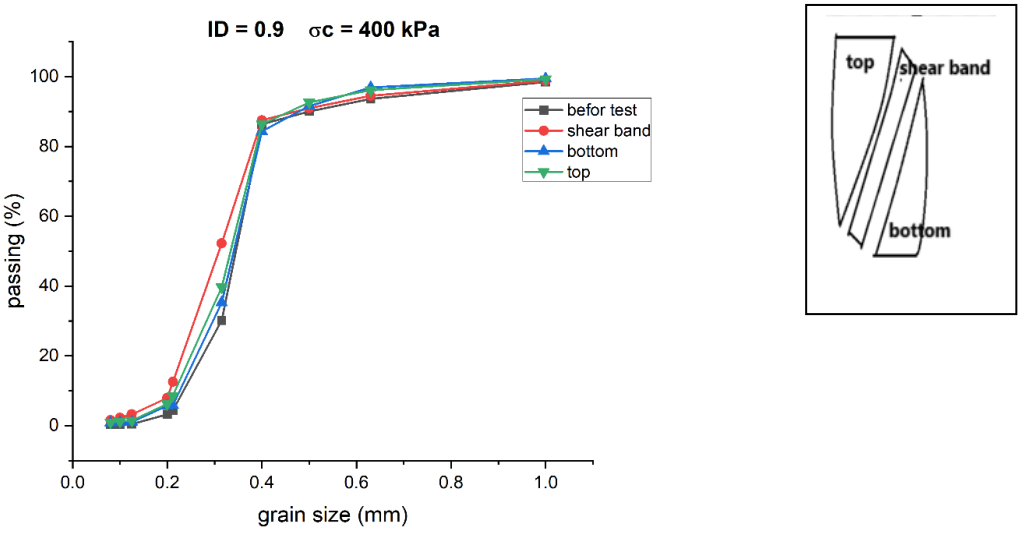

Fig. 9 Grain size distribution curves of 3 parts of OZ41 sand specimen sheared under confining pressure of 400 kPa.

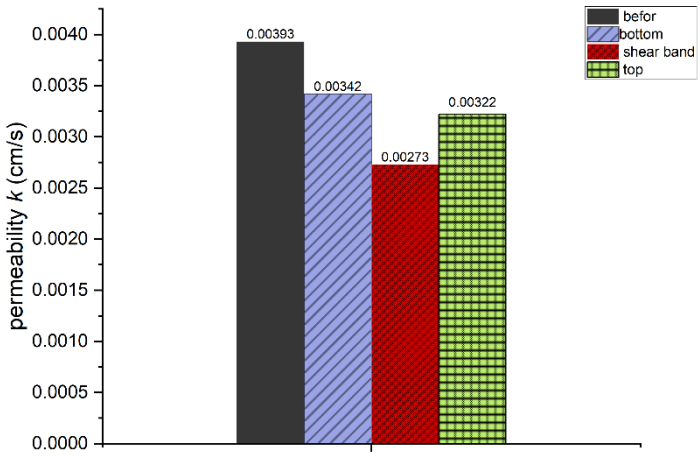

Fig. 10 Permeability in three parts of specimen sheared under confining pressure σ_c = 400 kPa.

The effect of grain damage on permeability is clearly visible in Figure 10, where the permeability coefficient (*k*) is lower in the shear band compared to the other two parts. This coefficient is higher in the bottom part compared to the top, consistent with the granulometry, which indicates a higher proportion of fine particles in the top part.

3.2. EFFECT OF VARIOUS PARAMETERS ON FINE PARTICLES PRODUCTION AND PERMEABILITY OF SHEARED SPECIMENS

3.2.1. EFFECT OF CONFINING PRESSURE

It is clear that the increase in confining pressure affects the production of fine particles. Grain size analyses carried out in the shear band of various specimens under different confining pressures (from 100 to 800 kPa), showed in Figure 11, clearly reveal an increase in fine particles with the rise in confining pressure. In Figure 12, the increase in the mass ration of fine particles (mf) to the total specimen mass (mt) is clearly observed. Rind et al. (2019) found the same results, in their series of tests conducted on sands subjected to different confining pressures.

The breakage mode can be observed in both Figures 13 and 14. It's manifested by abrasion under 100 kPa (the shape of grains becomes more rounded), and by fracture and abrasion under confining pressure 800 kPa. That explain the significant quantity of fine particles produced under this pressure value. This results in a rearrangement and compaction of particles leading to a deformation that is at least dilatant with increasing confining pressure.

By analyzing the differences in the percentage passing for each grain size before and after loading, it becomes evident that the breakage phenomenon mainly affects grains with a diameter close to the median diameter D50 (see Fig. 15), and does not affect those with larger diameter (Karatza et al., 2017).

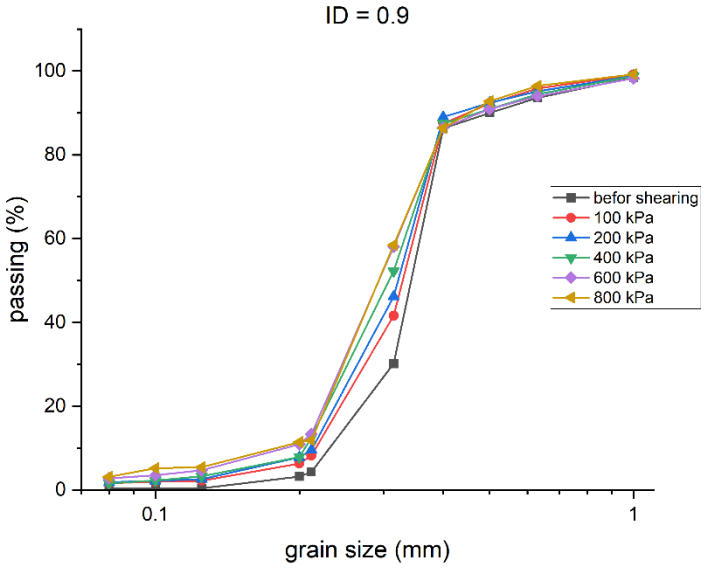

Fig. 11 Grain size distribution curves at shear band for dense sand ID 0.9 under σ_c=100, 200, 400, 600 and 800 kPa.

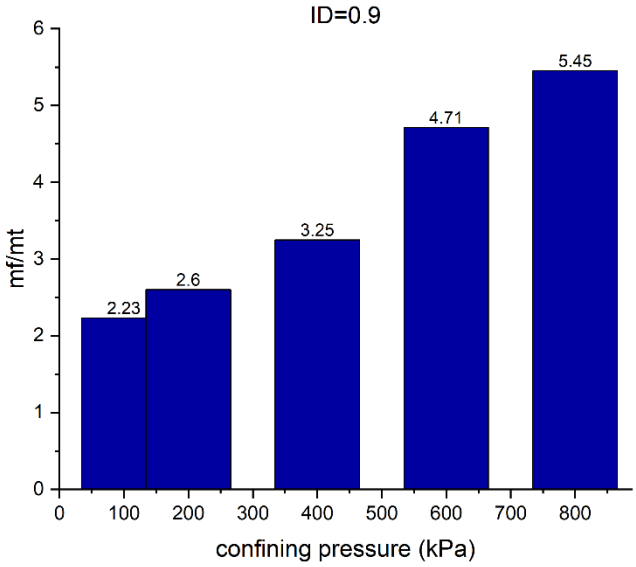

mt: Total mass of specimen mf: Fine particle mass

Fig. 12 Variation of passing percentage through the sieve 0.125 mm under different confining pressure.

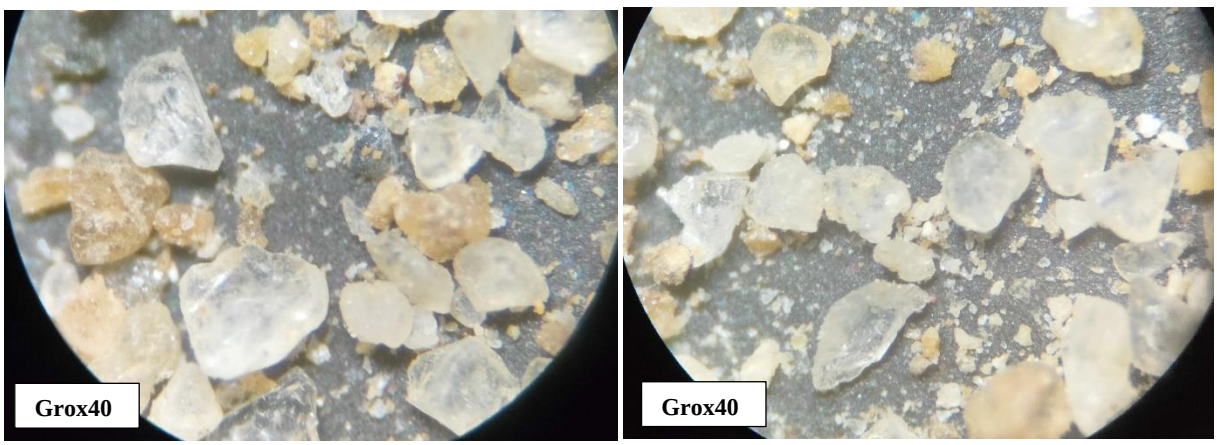

Fig. 13 Sand OZ81 after shear under confining pressure 800 kPa.

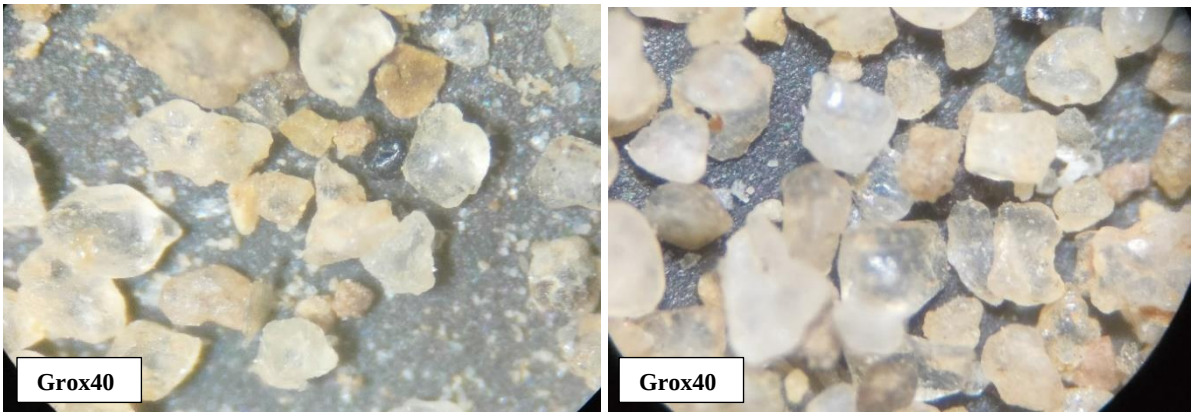

Fig. 14 Sand OZ11 after shear under confining pressure 100 kPa.

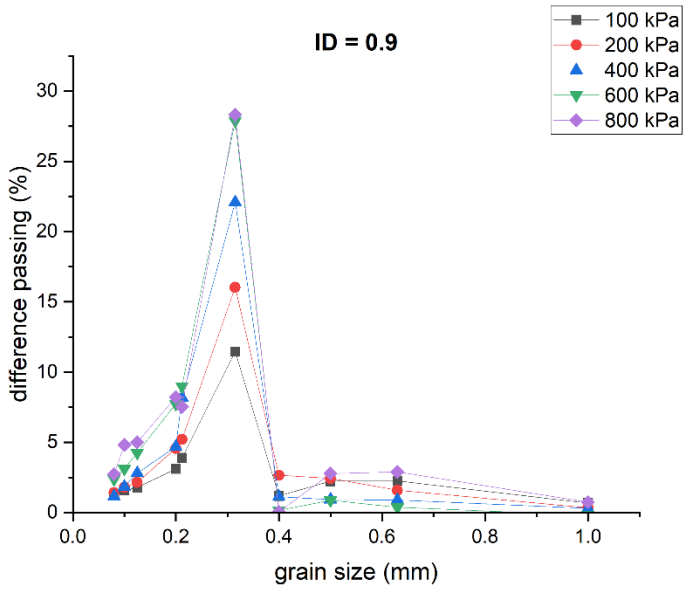

Fig. 15 Evolution of difference passing of grain size distribution under different confining pressures.

To quantify grain breakage, several quantitative measurements of the breakage rate have been proposed, to establish a quantitative parameter for comparison among different levels of rupture. These factors rely on changes in particle size as a key measure. Some are based on individual particle size between initial and final particle size distribution, such as those proposed by Marsal (1967), Lee and Farhoomand (1967), Lade et al. (1996), while others are based on changes in the overall distribution of particle size, as seen in Hardin (1985) and Einav (2007).

One area where breakage factors can have a significant application is permeability, there are many empirical correlations that link grain size with permeability, such as those developed by Hazen (1911), which relates permeability to diameter D_{10}.

Hattamleh et al (2013), based on the method developed by Lade et al (1996), were able to evaluate the quantity of fines particles by analyzing the evolution of grain size distribution curve under different confining pressure, calculating the breakage B_{10}:

$$B_{10}= (D_{10i} - D_{10f})/D_{10i} \quad (1)$$

Where

B_{10}: Breakage factor,

D_{10i}: Diameter of grains passing at 10 % of initial curve,

D_{10f}: Diameter of grains passing at 10 % of final curve,

Figure 16 illustrates the evolution of breakage factor, displaying a jump between 400 and 600 kPa of confining pressure, indicating more significant grain damage. As long as the curve has not stabilized, the quantity of fine particles increases with increasing confining pressure, suggesting that the fractal grain size distribution has not yet been reached.

The increase in confining pressure has led to greater grain damage, resulting in changes to the grain size distribution. This evolution in granulometry subsequently affects permeability. Rind et al. (2019) reported a reduction in permeability with increasing loading pressure, a trend previously observed by Feia et al. (2016). During consolidation, they noted that permeability declines with higher confining pressure.

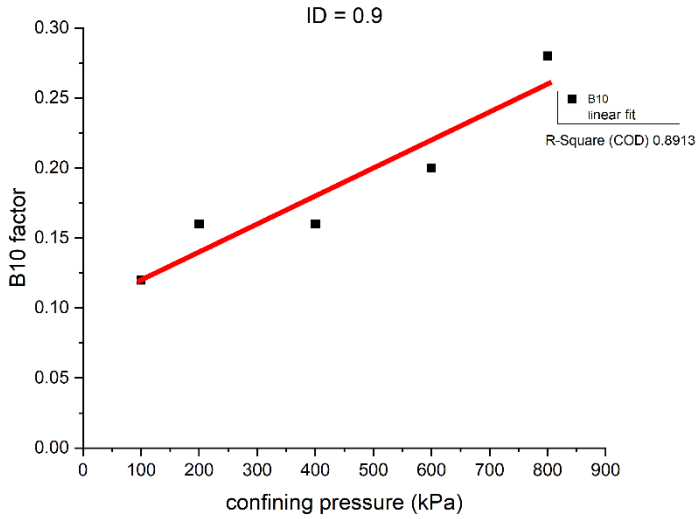

Fig. 16 Evolution of grain breakage as a function of confining pressure.

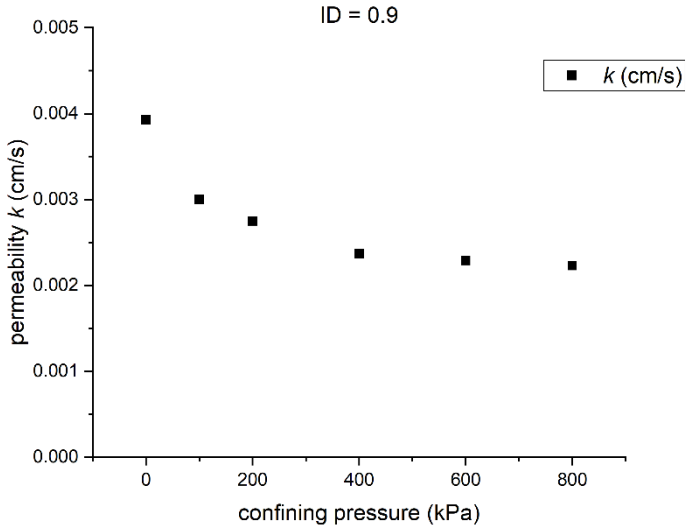

Fig. 17 Permeability *k* as a function of confining pressure during shearing.

The permeability measurements (see Fig. 17) similarly display a reduction as confining pressure rises, reaching a critical threshold around 600 kPa. This decrease is attributed to fine particles generated by grain damage in the shear band, as even minimal fine particles can significantly affect permeability.

Several researchers have attempted to relate permeability to various parameters such as porosity, grain size, and specific surface area. In the present study, we aimed to relate the permeability to changes in confining pressure. Figure 18 shows the variation of the permeability ratio (k/k_0) with confining pressure. Based on these data, an empirical relationship is derived within the pressure range of 0 to 600 kPa to describe the relationship between permeability and confining pressure.

The ratio of the permeability decreases with increasing confining pressure and can be fitted by the following equation:

$$\frac{k}{k_0} = e^{-b\sigma_c{}^n} \quad (2)$$

Where

n = 0.4 and b = 0.04

The permeability of a soil can also depends on grain size distribution. Hydraulic conductivity is known to be closely linked to pore structure, which is challenging to measure directly (Wang et al., 2017). However, since pore structure is inherently dependent on the soil's particle size distribution (PSD), empirical equations based on PSD remain a widely used approach for estimating hydraulic conductivity nowadays. The earliest empirical models for predicting hydraulic conductivity from particle size date back to the work of Hazen (1892) and Terzaghi (1925) (Shepherd, 1989; Wang et al., 2017). This highlights the crucial role of grain size in defining intrinsic permeability.

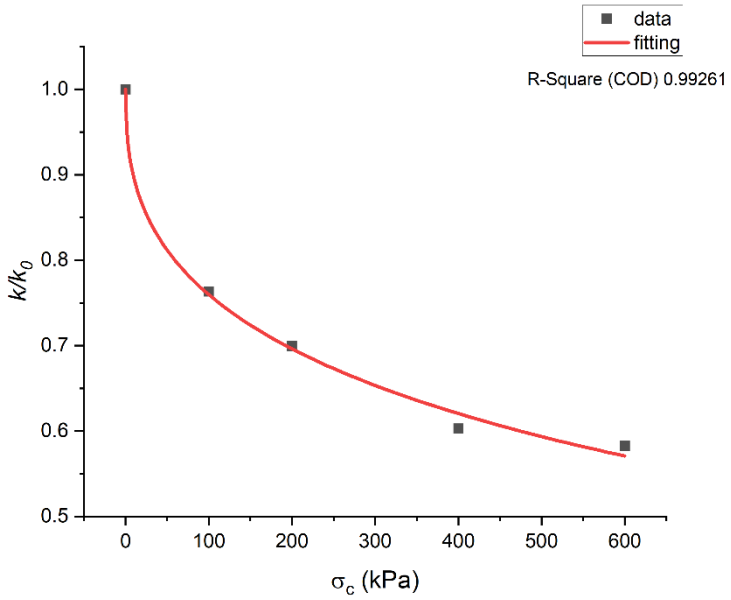

Fig. 18 Variation of the ratio of permeability (k/k_0) with the confining pressure.

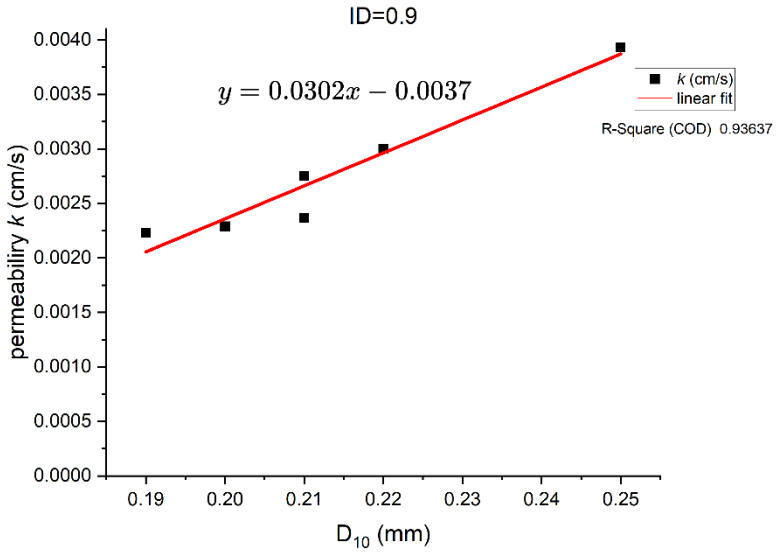

Fig. 19 Permeability k as a function of diameter D_{10}.

Hazen (1892) proposed an equation to estimate the permeability of loosely compacted sandy soils with a narrow grain size distribution (Philipponnat et al., 2011):

$$k = 1.25\ D_{10}^2 \quad (3)$$

Where k represents permeability in (cm/s), and D_{10} is the efficient grain diameter, defined as the particle size at which 10 % of the soil sample is finer.

In our case, for a dense sand, permeability increases with the diameter D_{10}, as shown in Figure 19.

Following this figure, an empirical relationship can be expressed by the following linear function:

$$k = 0.0302\ D_{10} - 0.0037 \quad (4)$$

Where k *is* the hydraulic conductivity (cm/s), D_{10} is the efficient diameter (mm). This relationship allows for an approximate estimation of the permeability of sand under specific conditions without resorting to laboratory tests that require more time.

This empirical law highlights an inverse relationship between permeability and the effective grain size D_{10}, which decreased from 0.25 mm to 0.19 mm as a result of a progressive change in the grain size distribution of an initially dense sand. This evolution stems from an increase in the fines content, generated by the progressive degradation of grains under varying confining pressures, leading to a microstructural reorganization and a reduction in porosity. These transformations significantly alter the connectivity and geometry of the pore network, which are key factors governing the material's hydraulic behaviour.

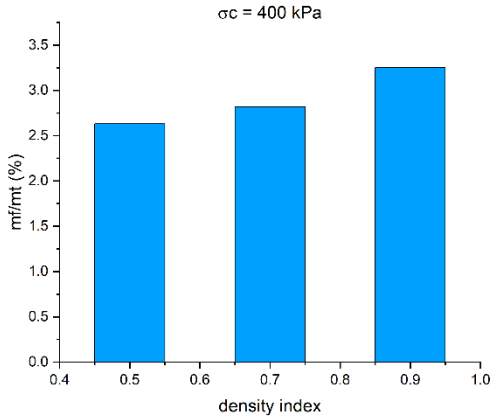

mt: Total mass of specimen mf: Fine particle mass

Fig. 20 Variation of produced fine particles for different density index.

Table 4 Friction angle of different sand.

ID	Friction Angle ϕ (°)
0.9	44
0.7	41
0.5	39

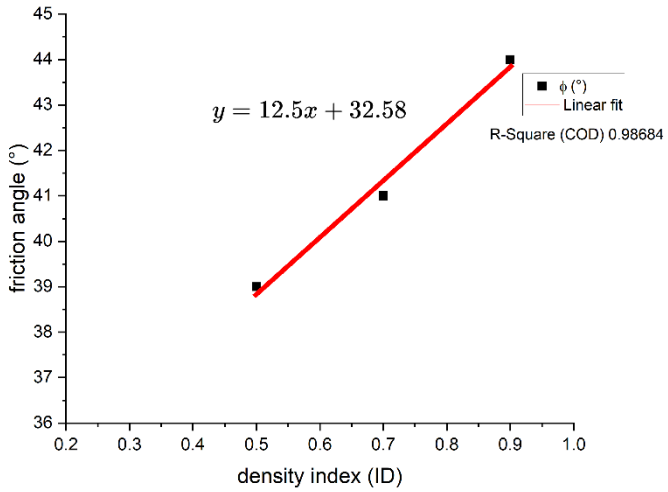

Fig. 21 Progress of friction angle versus density index.

This phenomenon reveals a coupled effect between the microstructure of the material and its hydraulic properties, placing this case in a markedly different context from that of classical permeability laws, which relate the hydraulic conductivity solely to the effective grain size D_{10}, in sands with intact, non-evolving granular structures and relatively constant porosity. Such models tend to overestimate permeability in conditions where the soil microstructure evolves under mechanical loading.

3.2.2. EFFECT OF DENSITY STATE

Grain breakage phenomenon is also affected by variations in sand density, with more significant grain damage observed in dense sand compared to medium-density sand, resulting of higher friction between the sand grains in dense sand (friction angle ϕ = 44°), compared to medium density sand (friction angle ϕ = 39°), (see Table 4). It should be noted that the friction angle increases with increasing density index. Delage et al. (2017) found the same results in their study conducted on regolith simulant sands from the Martian soil, confirming the important effect of density on the friction angle.

Based on these available data (showed in Fig. 21) the friction angle can be written as the following equation:

$$\varphi(°) = 12.5I_D + 32.58 \quad (5)$$

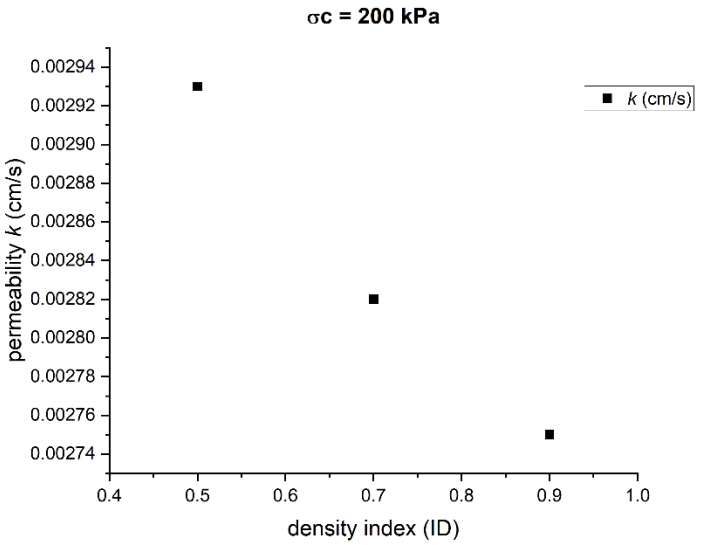

Fig. 22 Evolution of permeability *k* as a function of density index ID.

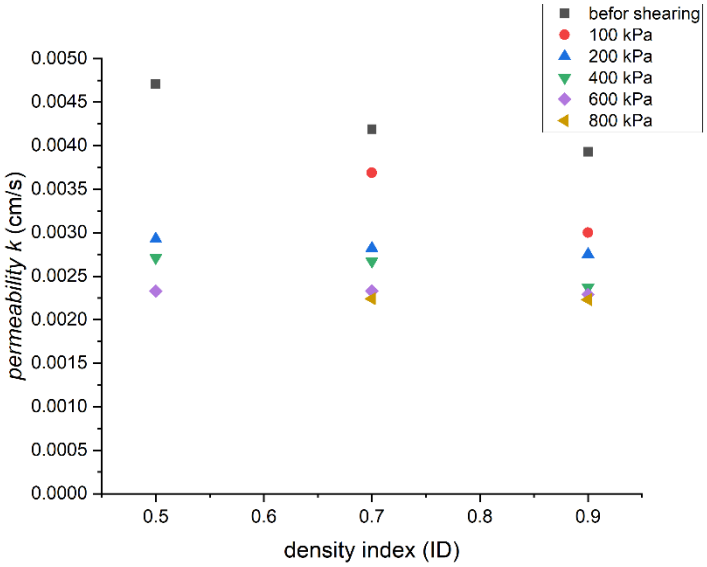

Fig. 23 Variation of the permeability *k* as a function of density index ID.

A decrease in permeability is also observed with an increase in density index (see Fig. 22), confirming that grain damage increases with higher density. However, this permeability becomes insensitive to changes in the density state (see Fig. 23), as an increase in confining pressure suppresses the density effect. The decrease in permeability with increasing density index shows a steeper slope before shearing and at 100 kPa compared to the other pressures, where the slope of the variation becomes almost zero at 600 and 800 kPa.

In this context, the behavior of permeability under varying density and confining pressure illustrates how these factors interact in granular soils. Initially, as the density index increases, permeability changes more rapidly with confining pressure, resulting in a steep regression slope both before and after shear. For lower pressures such as 100 kPa, density is more influential, as grains can still adjust relative to each other, impacting permeability. However, at higher confining pressures (600-800 kPa), the slope flattens significantly, approaching a horizontal line. This suggests that at high confining pressures and with grain fragmentation, the effect of density on permeability diminishes, as the soil structure becomes compacted enough to limit further influence from density changes. A similar phenomenon is observed with fine particles content (see Fig. 24) where permeability becomes insensitive to an increase in fine particles beyond a certain value. As noted by Boadu (2000), where an increase in fine particles beyond a critical threshold leads to disconnection or loss of contact between sand grains. The coarse particles become dispersed within a fines-dominated matrix.

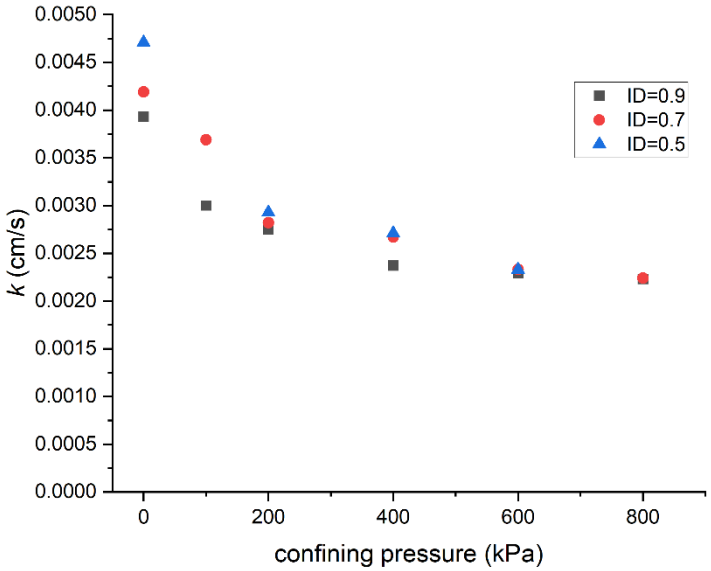

Fig. 24 Evolution of permeability *k* as a function of fine particles content of different densities of sand (ID 0.9, ID 0.7 et ID 0.5).

4. CONCLUSION

An experimental study based on consolidated drained (CD) triaxial tests was conducted to explore grain breakage and its effect on mechanical behavior and permeability of silica-sand, under various confining pressure. Three different densities were chosen (medium ID = 0.5, moderately dense ID = 0.7, and dense ID = 0.9) to study the influence of this parameter on grain breakage, several measurements were taken during for each test under different confining pressure.

The experimental results demonstrate that the increase in density index significantly affects the grain breakage, which becomes more pronounced with increasing confining pressure, leading to an evolution of the initial sand grain size distribution. After freezing the sheared sample, granulometric tests performed on three parts of the sample revealed that fines particles production due to grain breakage is primarily localized within shear band. This localized fragmentation explains the decrease in permeability observed during the triaxial test, as reported in similar studies.

For a better understanding this phenomenon, the investigation focused on the shear band with the implementation of various tests, providing the following explanations. The continuous increase in breakage factor B_{10} suggests that fractal granulometry has not yet been reached and its progression will continue with increasing confining pressure. Grain breakage, concentrated mainly within the shear band, predominantly affects particles with diameters close to the median diameter D_{50}, while leaving larger particles unaffected as they are shielded by the smaller ones.

Various permeability tests were conducted on the shear band for each sand specimen sheared at different density index and under various confining pressure. The results indicate even with a small quantity of fine particles produced a decrease in the permeability coefficient with an increase in the density index, as well as confining pressure, until critical threshold, beyond this threshold obtained at 600 kPa, the *k* value becomes insensitive to changes in the density state, where the increase in confining pressure leads to the suppression of the density effect.

The experimental relationship established within the pressure range of 0 to 600 kPa can be useful for estimating the permeability of dense granular materials without the need for additional experiments, provided the initial permeability and the confining pressure to which they will be subjected are known. This has practical benefits for engineers designing underground storage facilities, tunneling projects, and other subsurface structures where permeability plays a critical role in performance and safety.

DISCLOSURE STATEMENT

No potential conflict of interest was reported by the authors.

DATA AVAILABILITY STATEMENT

The authors confirm that the data supporting the findings of this study are available within the article.

REFERENCES

Alikarami, R., Andò, E., Gkiousas-Kapnisis, M., Torabi, A. and Viggiani, G.: 2015, Strain localization and grain breakage in sand under shearing at high mean stress: insights from in situ X-ray tomography. Acta Geotechnica, 10(1), 15–30. DOI: 10.1007/s11440-014-0364-6

Andò, E., Viggiani, G., Hall, S.A. and Desrues, J.: 2013, Experimental micro-mechanics of granular media studied by x-ray tomography: Recent

results and challenges. Geotechnique Letters, 3, 142–146. DOI: 10.1680/geolett.13.00036

Arslan, H., Baykal, G. and Sture, S.: 2009, Analysis of the influence of crushing on the behavior of granular materials under shear. Granular Matter, 11(2), 87–97. DOI: 10.1007/s10035-009-0127-5

Boadu, F.K.: 2000, Hydraulic Conductivity of Soils from Grain-Size Distribution: New Models. Journal of Geotechnical and Geoenvironmental Engineering, 126(8), 739–746. DOI: 10.1061/(ASCE)1090-0241(2000)126:8(739)

Bolton, M.D., Nakata, Y. and Cheng, Y.P.: 2008, Micro- and macro-mechanical behaviour of DEM crushable materials. Geotechnique, 58(6), 471–480. DOI: 10.1680/geot.2008.58.6.471

Coop, M.R., Sorensen, K.K., Bodas Freitas, T. and Georgoutsos, G.: 2004, Particle breakage during shearing of a carbonate sand. Geotechnique,54, 3 157–163. DOI: 10.1680/geot.2004.54.3.157

Delage, P., Karakostas, F., Dhemaied, A., Belmokhtar, M., Lognonné, P., Golombek, M., de Laure, E., Hurst, K., Dupla, J.C., Kedar, S., Cui, Y.J. and Banerdt, B.: 2017, An investigation of the mechanical properties of some martian regolith simulants with respect to the surface properties at the insight mission landing site. Space Sci. Rev., 211, 1–4, 191–213. Springer Netherlands. DOI: 10.1007/s11214-017-0339-7

Einav, I.: 2007, Breakage mechanics-Part I: Theory. Journal of the Mechanics and Physics of Solids, 55(6), 1274–1297. DOI: 10.1016/j.jmps.2006.11.003

Feia, S., Sulem, J., Canou, J., Ghabezloo, S. and Clain, X.: 2016, Changes in permeability of sand during triaxial loading: effect of fine particles production. Acta Geotechnica, 11(1), 1–19. DOI: 10.1007/s11440-014-0351-y

Hardin, B.: 1985, Crushing of Soil Particles. ASCE Journal of Geotechnical Engineering, 111, 10, 1177–1192. DOI: 10.1061/(ASCE)0733-9410(1985)111:10(1177)

Hattamleh, O.H., Al-Deeky, H.H. and Akhtar, M.N.: 2013, The Consequence of Particle Crushing in Engineering Properties of Granular Materials. International Journal of Geosciences, 4(7), 1055–1060. DOI: 10.4236/ijg.2013.47099

Karatza, Z.: 2018, A study of temporal and spatial evolution of deformation and breakage of dry granular materials using x-ray computed tomography and the discrete element method. Ph.D. Thesis, The University of Edinburgh.

Karatza, Z., Andò, E., Papanicolopulos, S.A., Ooi, J.Y. and Viggiani, G.: 2017, Evolution of deformation and breakage in sand studied using X-ray tomography. Geotechnique, 68(2), 107–117. DOI: 10.1680/jgeot.16.P.208

Karatza, Z., Andò, E., Papanicolopulos, S.A., Ooi, J.Y. and Viggiani, G.: 2019, Effect of particle morphology and contacts on particle breakage in granular assembly studied using X-ray tomography. Granular Matter, 21(3), 44. DOI: 10.1007/s10035-019-0898-2

Kikumoto, M., Muir, D. and Russell, A.: 2010, Particle crushing and deformation behaviour. Soils and foundations, 50, 4, 547–563. DOI: 10.3208/sandf.50.547

Lade, P.V., Yamamuro, J.A. and Bopp, P.A.: 1996, Significance of particle crushing in granular materials. Journal of Geotechnical Engineering, 122(4), 309–316. DOI: 10.1061/(ASCE)0733-9410(1996)122:4(309)

Lee, K.L. and Farhoomand, I.: 1967, Compressibility and crushing of granular soils in anisotropic triaxial compression. Can. Geotech. J., 4(1), 68–86. DOI: 10.1139/t67-012

Marsal, R.J.: 1967, Large scale testing of rockfill materials. Journal of the Soil Mechanics and Foundation Division. 93(2), 27–43. DOI: 10.1061/JSFEAQ.0000958

Masch, F.D. and Denny, K.J.: 1966, Grain size distribution and its effect on the permeability unconsolidated sands, Water Resources Research, 2, 4, 665–677. DOI: 10.1029/WR002i004p00665

Ovalle, C., Dano, C. and Hicher, P.-Y.: 2013, Experimental data highlighting the role of surface fracture energy in quasi-static confined comminution. International Journal of Fracture Mechanics, 182(1), 123–130. DOI: 10.1007/s10704-013-9833-4

Ovalle, C.: 2013, Contribution to the study of grain breakage in granular materials. Ph.D. thesis, École Centrale de Nantes, France, (in French),

Philipponat, G. and Hubert, B.: 2011, Foundations and earth structures. EYROLLES Publishing. (in French).

Rind, T.A., Zulfiqar, S., Campus, A.B., Mirs, K., Karira, H., Jhatial, A.A., Sohu, S., Sandhu, A.R., Ali, Z. and Campus, B.: 2019, Particle crushing effect on the geotechnical properties of soil. Eng. Technol. Appl. Sci. Res., 9, 3.

Salami, Y., Dano, C., Hicher, P.-Y. and Alonso, E.: 2015, Thermomechanical approach for modeling the behavior of soils affected by grain breakage., (in French). https://hal.archives-ouvertes.fr/hal-01167691

Sammis, C., Osborne, R., Anderson, J., Banerdt, M. and White, P.: 1986, Self-similar cataclasis in the formation of fault gouge. Pure and Applied Geophysics, 124(1-2), 53–78. DOI: 10.1007/BF00875719

Shepherd, R.G.: 1989, Correlations of permeability and grain size. Ground Water, 27(5), 633–638. DOI: 10.1111/j.1745-6584.1989.tb00476.x

Turcotte, D.L.: 1986, Fractals and fragmentation. Journal of Geophysical Research, 91(B2), 1921–1926. DOI: 10.1029/JB091iB02p01921

Wang, J.F., Yan, H.B.: 2011, 3D DEM simulation of crushable granular soils under plane strain compression condition. Procedia Engineering. 14, 1713–1720. DOI: 10.1016/j.proeng.2011.07.215

Wang, J.P., François, B. and Lambert, P.: 2017, Equations for hydraulic conductivity estimation from particle size distribution: A dimensional analysis. Water Resources Research, 53(9), 8127–8134. DOI: 10.1002/2017WR020888

Wu, M. and Wang, J.: 2021, Estimating contact force chains using artificial neural network. Applied Sciences, 11(14), 6278. DOI: 10.3390/app11146278

Zhao, B., Wang, J., Coop, M.R., Viggiani, G. and Jiang, M.: 2015, An investigation of single sand particle fracture using x-ray micro-tomography. Geotechnique, 65(8), 625–641. DOI: 10.1680/geot.4.P.157